

NASA-TM-83650

DOE/NASA/1005-3  
NASA TM-83650

NASA-TM-83650

19840016441

# Comparison of Free-Piston Stirling Engine Model Predictions with RE1000 Engine Test Data

Roy C. Tew  
National Aeronautics and Space Administration  
Lewis Research Center

LIBRARY COPY

JUN 5 1984

LANGLEY RESEARCH CENTER  
LIBRARY, NASA  
HAMPTON, VIRGINIA

Work performed for  
**U.S. DEPARTMENT OF ENERGY**  
**Conservation and Renewable Energy**  
**Division of Building and Community Systems**

Prepared for  
Nineteenth Intersociety Energy Conversion Engineering Conference  
cosponsored by the ANS, ASME, SAE, IEEE, AIAA, ACS, and AIChE  
San Francisco, California, August 19-24, 1984

## DISCLAIMER

This report was prepared as an account of work sponsored by an agency of the United States Government. Neither the United States Government nor any agency thereof, nor any of their employees, makes any warranty, express or implied, or assumes any legal liability or responsibility for the accuracy, completeness, or usefulness of any information, apparatus, product, or process disclosed, or represents that its use would not infringe privately owned rights. Reference herein to any specific commercial product, process, or service by trade name, trademark, manufacturer, or otherwise, does not necessarily constitute or imply its endorsement, recommendation, or favoring by the United States Government or any agency thereof. The views and opinions of authors expressed herein do not necessarily state or reflect those of the United States Government or any agency thereof.

Printed in the United States of America

Available from

National Technical Information Service  
U.S. Department of Commerce  
5285 Port Royal Road  
Springfield, VA 22161

NTIS price codes<sup>1</sup>

Printed copy: A02

Microfiche copy: A01

<sup>1</sup>Codes are used for pricing all publications. The code is determined by the number of pages in the publication. Information pertaining to the pricing codes can be found in the current issues of the following publications, which are generally available in most libraries: *Energy Research Abstracts (ERA)*; *Government Reports Announcements and Index (GRA and I)*; *Scientific and Technical Abstract Reports (STAR)*; and publication, NTIS-PR-360 available from NTIS at the above address.

DISPLAY 32/2/1

84N24509\*# ISSUE 14 PAGE 2249 CATEGORY 85 RPT#: NASA-TM-83650  
E-2095 DOE/NASA/1005-3 NAS 1.15:83650 CNT#: DE-AI05-820R-1005 84/00/00  
21 PAGES UNCLASSIFIED DOCUMENT

UTTL: Comparison of free-piston Stirling engine model predictions with RE1000  
engine test data

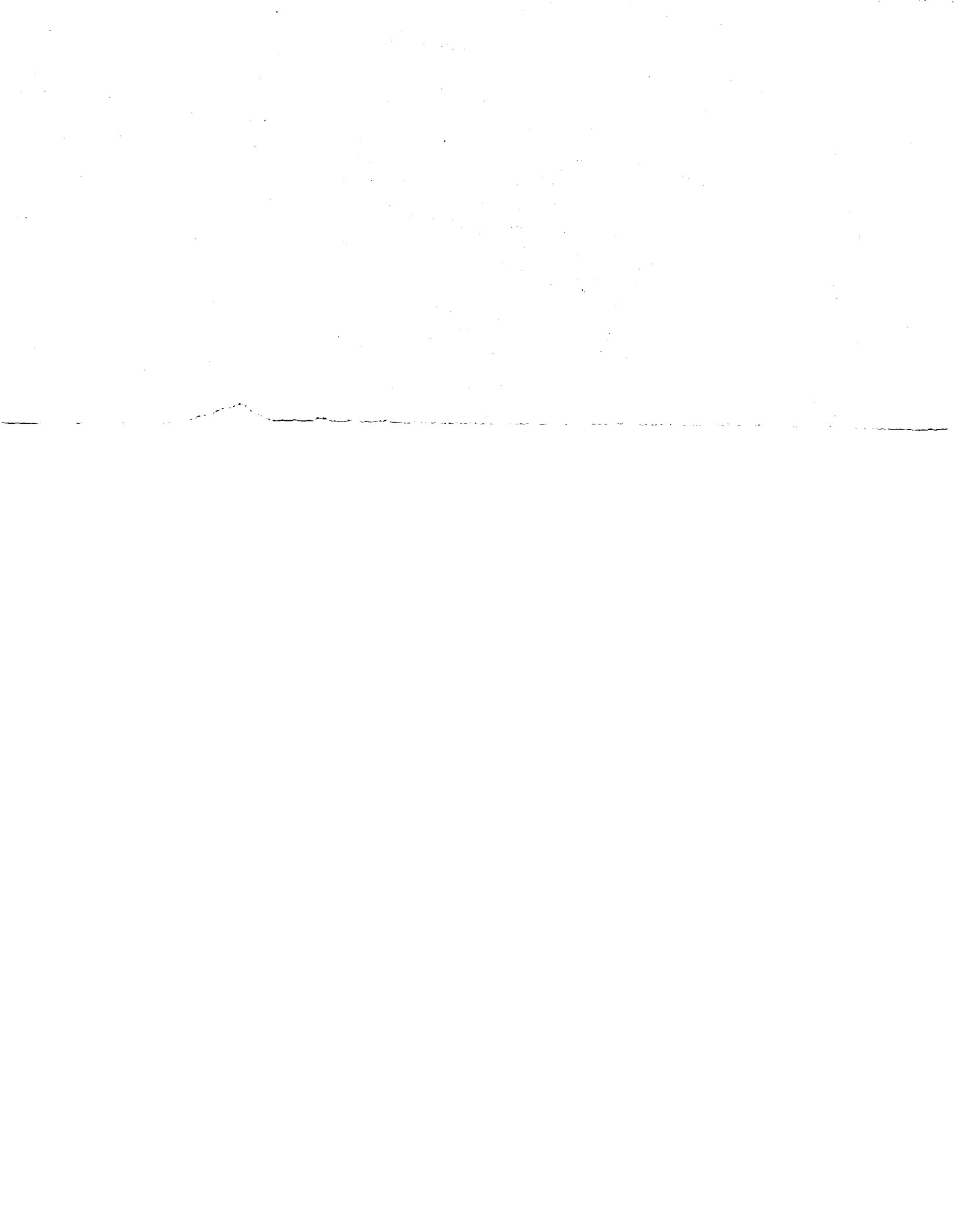
AUTH: A/TEW, R. C.

CORP: National Aeronautics and Space Administration, Lewis Research Center,  
Cleveland, Ohio. AVAIL.MTIS SAP: HC A02/MF A01

Proposed for presentation at the 19th Intersoc. Energy Conversion Eng.  
Conf., San Francisco, 19-24 Aug. 1984; sponsored by American Nuclear  
Society, ASME, SAE, IEEE, AIAA, ACS, and AIChE

MAJS: /\*COMPUTERIZED SIMULATION/\*MATHEMATICAL MODELS/\*PERFORMANCE PREDICTION/\*  
PISTONS/\*PROGRAM VERIFICATION (COMPUTERS)/\*STIRLING CYCLE





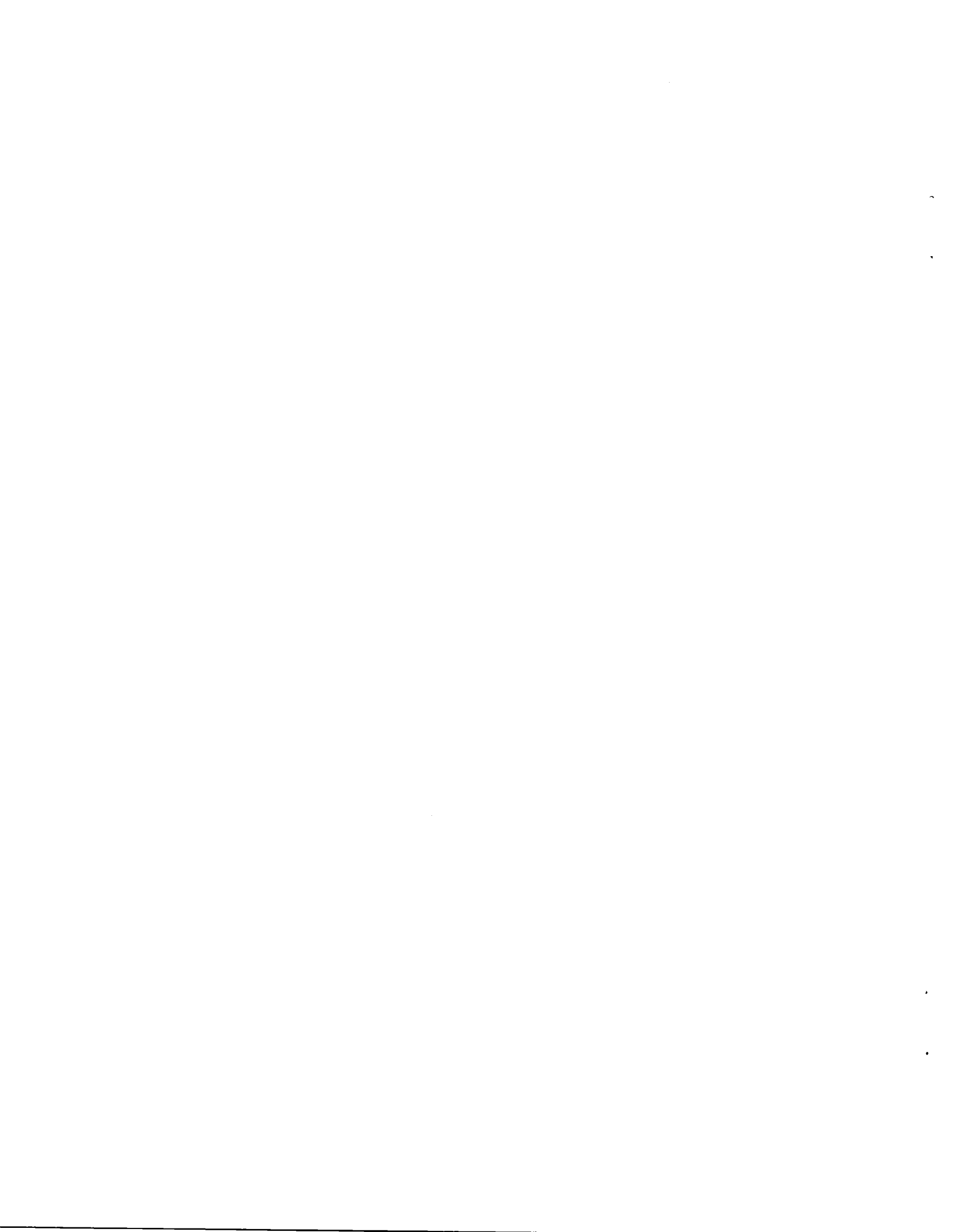
# **Comparison of Free-Piston Stirling Engine Model Predictions with RE1000 Engine Test Data**

Roy C. Tew  
National Aeronautics and Space Administration  
Lewis Research Center  
Cleveland, Ohio 44135

Work performed for  
U.S. DEPARTMENT OF ENERGY  
Conservation and Renewable Energy  
Division of Building and Community Systems  
Washington, D.C. 20545  
Under Interagency Agreement DE-AI05-82OR1005

Prepared for  
Nineteenth Intersociety Energy Conversion Engineering Conference  
cosponsored by the ANS, ASME, SAE, IEEE, AIAA, ACS, and AIChE  
San Francisco, California, August 19-24, 1984

N84-24509#



COMPARISON OF FREE-PISTON STIRLING ENGINE MODEL PREDICTIONS WITH RE1000 ENGINE TEST DATA

Roy C. Tew  
National Aeronautics and Space Administration  
Lewis Research Center  
Cleveland, Ohio 44135

ABSTRACT

Predictions of a free-piston Stirling engine model are compared with RE1000 Sunpower engine test data taken at NASA-Lewis Research Center. The model validation and the engine testing are being done under a joint inter-agency agreement between the Department of Energy's Oak Ridge National Laboratory and NASA Lewis.

A kinematic code developed at Lewis was upgraded by Mechanical Technology, Inc. to permit simulation of free-piston engine performance; it was further upgraded and modified at Lewis and is currently being validated. The model predicts engine performance by numerical integration of equations for each control volume in the working space. Piston motions are determined by numerical integration of the force balance on each piston or can be specified as Fourier series. In addition, the model Fourier analyzes the various piston forces to permit the construction of phasor force diagrams. The paper compares predicted and experimental values of power and efficiency and shows phasor force diagrams for the RE1000 engine displacer and piston.

Further development plans for the model are also discussed.

SYMBOLS

$A_{dis}$	displacer cross-sectional area (0.6065 cm <sup>2</sup> )
$A_{pis}$	piston cross-sectional area (0.6180 cm <sup>2</sup> )
$A_{rod}$	displacer rod cross-sectional area (0.05224 cm <sup>2</sup> )
$C_d$	damping constant for displacer gas spring
$C_{load}$	dashpot load constant
$dV$	differential volume
$F_{spring}$	net spring force
$K_d$	spring constant for displacer gas spring
$M_d$	displacer mass (0.4259 kg)

$M_p$	piston mass (6.200 kg)
$P$	pressure
$P_b$	buffer space pressure amplitude
$P_e$	expansion space pressure amplitude
$P_c$	compression space pressure amplitude
$\Delta P, P_e - P_c$	pressure drop across displacer
$t$	time in the form of Fourier series
$x_d, \dot{x}_d, \ddot{x}_d$	displacer amplitude, velocity, acceleration
$x_p, \dot{x}_p, \ddot{x}_p$	piston amplitude, velocity, acceleration
$\omega$	engine frequency
$\phi$	power piston-compression space pressure phase angle

INTRODUCTION

This paper summarizes the progress made on the development and validation of a free-piston Stirling engine performance computer code. Plans for continued development of the model are also discussed.

Under a contract with Lewis Research Center, Mechanical Technology, Inc. (MTI) upgraded a Lewis developed kinematic code (1) and (2) to permit simulation of free-piston Stirling engines. The resulting upgraded code was used to model the 1 kW Department of Energy Demonstrator Engine (3) which was being tested at MTI; Although a few predictions were made with the code for comparison with test data, the code was not validated due to a lack of contract funds. Documentation of the upgraded code was prepared for Lewis (4).

Development of this code is proceeding at Lewis under an interagency agreement between NASA-Lewis and the Department of Energy's Oak Ridge National Laboratory. Under this

E-2095

agreement an RE1000 Sunpower, Inc. engine has been modeled. Engine testing is ongoing and predictions of the model are being checked against test data.

The RE1000 free-displacer, free-piston engine produces a nominal 1 kW of power. A complete description of the engine plus some initial results of the Lewis tests are given in Ref. 5; this initial test data showed that the performance of the engine at Lewis was poorer than observed during acceptance testing at Sunpower. Reference 6 explains how these engine performance problems were solved and contains test data taken after engine and test rig modifications were made to improve performance; this second set of test data was used in this paper for comparison with the RE1000 model predictions.

The procedure used in comparing the model predictions with test data was to calibrate the model against one data point and then generate a range of predictions for various loads (at two different hot end temperatures). The use of phasor diagrams to compare predicted and experimental pressure variations, displacer motions, and piston motions was a key element of the calibration procedure. The parameters used to calibrate the model were those considered to be difficult to specify accurately from engine geometrical data. It is expected that, as several deficiencies in the model are corrected and parameters, such as pressure drop, are more accurately known from experimental data, less calibration will be required.

While the free-piston code was being developed, the kinematic code of Refs. 7 and 8 was being independently upgraded at Lewis Research Center (this upgraded kinematic code is now available from NASA's Computer Software and Information Center (COSMIC)); some of the features incorporated in the this upgraded kinematic code--complete cooler model, appendix gap pumping loss, adiabatic connecting ducts--should be incorporated in the free-piston code.

#### ENGINE DESCRIPTION

A detailed description of the engine, including engine dimensions and parameters used in simulating the engine, is given in Ref. 5. Many schematics and photographs of the engine and its components are shown in Ref. 5 and 6.

A cutaway view of the RE1000 engine is shown in Fig. 1. The dashpot load is adjusted by varying the opening of a valve which regulates the flow of gas between the dashpot cylinder and the buffer space; the buffer space is the gas volume located over the power

piston, as shown in Fig. 1, and surrounding the dashpot cylinder. The dashpot is modeled as a load which is proportional to the square of the power piston velocity.

The schematic of Fig. 2 shows how the displacer rod is attached, via the "spider", to the wall; thus the displacer gas spring is referenced to ground. The path through the displacer rod and spider allows the displacer gas spring to communicate with the buffer space when the centerports in the rod and its sleeve are aligned. The primary leakage path for the displacer gas spring is by the displacer rod and via the centerport flow path to the buffer space.

Figure 3 shows the simulated leakage path from the compression space along the power piston, to the power piston centerport. Not shown in this figure is the centerport flow path through the power piston (from the compression space to the centerports). Photographs of the cooler in Ref. 5 show the rectangular slots through which the working gas flows and the cylindrical flow passages in the aluminum cooler housing through which the coolant flows.

#### MODEL DESCRIPTION

Both the original kinematic code and the derived free-piston code share the following general characteristics: Engine power and efficiency are predicted for a given set of engine operating conditions (mean pressure, boundary temperatures engine speed for the kinematic code, and engine load for the free-piston code.) The working space model includes the motion of a power piston and displacer, swept volumes--the expansion and compression spaces, and three heat exchangers--heater, regenerator and cooler--connected in series between the two swept volumes. The working space is divided into a number of control volumes for analysis of fluid flow and heat transfer. Flow resistances and heat transfer coefficients are calculated for each control volume at each time step over the engine cycle. Within each control volume the continuity and energy equations are numerically integrated with respect to time; a simplified momentum equation (pressure drop is a function of flow rate and friction factor) and an equation of state are also used in the calculations. Thus in addition to overall performance, the cyclic variations in the working space variables--pressure, volume, temperatures and flow rates are calculated. In general, the same thermodynamic solution techniques are used in both the original kinematic code (as documented in ref. 1) and in the free-piston code.

The free-piston code includes the following changes relative to the original kinematic code of Ref. 1:

1. Equations of motion for piston and displacer were incorporated with an option to run in either constrained (kinematic) or unconstrained (free-piston) modes.

2. Centering ports, for centering piston and displacer motions were modeled.

3. Leakage paths along the power piston and displacer rods were modeled.

4. The model was set up to allow the choice of several different types of loads when operating in the unconstrained mode (dashpot, linear alternator, hydraulic output).

5. A Fourier analysis subroutine was added so that a number of engine variables are now routinely Fourier analyzed.

6. Simpson rule integration was substituted for trapezoidal integration to improve the accuracy of the work calculation and allow reduction of the number of time steps per engine cycle.

7. A number of additional modifications were made with the object of making the code more flexible. Engine dimensions, operating conditions, and model parameters and option indicies were all collected together in an input dataset. The number of control volumes in each of the three heat exchangers was made independently specifiable in the input dataset. The code was made more modular (more subroutines are now used).

Since the validation effort at Lewis has begun, some changes in the model configuration were required to model the RE1000 engine (For example the DOE Demonstrator Engine has a power piston gas spring; the RE1000 engine does not). Additional modifications were made to the code to improve the overall convergence to a solution. A subroutine was added to calculate phasor magnitudes and phases (from the Fourier analyzed engine variables). Use of these phasors to construct engine phasor diagrams is equivalent to approximating the engine dynamics by a linearized model; such diagrams helped in understanding the effect of various model modifications on predicted engine performance and were useful in calibration of the model.

#### APPROACH

It was necessary to calibrate the model for operation in the unconstrained (free displacer and piston) mode. Calibration was

accomplished by adjustment of several model parameters which are difficult to specify accurately from geometrical data, namely: dashpot load constant, centerport flow coefficients for piston and displacer, displacer gas spring and power piston leakage factors, and pressure drop multiplication factor. These adjustments were made, primarily, with the model operating in the constrained mode (that is with input displacer and piston motions).

For the constrained model runs, the input motions for piston and displacer were Fourier analyzed test data; the Fourier analysis was carried out to the third harmonic term. For the unconstrained model runs, the motion of each piston was determined by integration of Newton's equation of motion.

The experimental case selected for model calibration was Run #495 (this was a recent test run and was not reported on in ref. 5 and 6); the operating conditions for this run were:

Heater Temperature = 600° C

Coolant Inlet Temperature = 30° C

Mean Pressure = 7.0 MPa (1015 psi)

Helium was the working fluid used in the engine. The dashpot load imposed at the above conditions determined the piston, displacer and pressure amplitudes and the engine frequency of 30.4 Hz (frequency is not very sensitive to changes in load). These experimental amplitudes and their relative phasing were then used, along with the test values of power and efficiency, in calibrating the model. The above operating conditions will be referred to as the Reference Case operating conditions. In making predictions, the model cooler wall temperature was set equal to the measured coolant inlet temperature.

The procedure used in adjusting the calibration parameters was to match:

1. The modeled load with the experimental load (accomplished by adjusting the dashpot power dissipation to agree with the power into the constrained motion piston.)

2. The predicted pressure variation with the experimental pressure variation.

3. The predicted displacer force balance with the force balance required to produce the experimental displacer motion.

Adjustments were made with the model operating in the constrained mode; the model was then run in the unconstrained mode to see if its predictions still agreed well with the test data. Actually, several iterations between

constrained and unconstrained modes were required to complete the calibration.

The set of calibration parameters which best matched the modeled load and performance to the Reference Case test data was:

$$\text{Dashpot load constant} = 1.724\text{E-}2 \text{ N-sec}^2/\text{cm}^2 \\ (2.5\text{E-}2 \text{ lbf-sec}^2/\text{in}^2)$$

$$\text{Piston centerport flow coefficient} = 28.0\text{E-}3$$

$$\text{Displacer centerport flow coefficient} = \\ 1.0\text{E-}03$$

$$\text{Displacer spring leakage factor} = 0.2$$

$$\text{Power piston leakage factor} = 1.2$$

$$\text{Pressure drop multiplication factor} = 3.0$$

The above set of parameters was used in the rest of the study.

#### COMPARISON OF PREDICTIONS WITH REFERENCE CASE TEST DATA

Figures 4 to 7 are phasor diagrams which show, approximately, the amplitudes and phase relationships of the calibrated model variables and the measured Reference Case pressure; diagrams are shown for constrained and unconstrained model predictions. All phasors are plotted with phase relative to the piston amplitude. Both piston amplitude,  $X_p$ , and displacer amplitude,  $X_d$ , are considered positive for displacements toward the hot end of the engine. Zero displacements occur when the respective centerports of the displacer gas spring and power piston are aligned with the centerport flow paths.

For the simulation represented by Fig. 4 and 5, measured piston and displacer motions were input to the model. The inputs were in the form of Fourier series as shown below (amplitudes are in centimeters):

$$X_p = 0.170 + 1.309 \sin \omega t \\ + 0.019 \sin (2\omega t + 55.53^\circ) \\ + 0.010 \sin (3\omega t + 97.52^\circ)$$

$$X_d = -0.120 + 1.188 \sin (\omega t + 50.86^\circ) \\ + 0.030 \sin (2\omega t + 89.9^\circ) \\ + 0.024 \sin (3\omega t + 39.45^\circ)$$

The piston and displacer phasors shown in Fig. 4 represent only the fundamentals of the measured motion, but it is seen that the amplitudes of the higher order terms are small.

The dashed line pressure phasor in the diagrams (1.101 MPa @ -17.7°) phase relative to the piston amplitude) represents the fundamental from the following Fourier series; this series was determined by analysis of the measured compression space pressure variation (units in MPa):

$$P_c = -0.082 + 1.101 \sin (\omega t - 17.7^\circ) \\ + 0.082 \sin (2\omega t - 128^\circ) \\ + 0.002 \sin (3\omega t - 138^\circ)$$

The solid line, predicted pressure phasor for constrained motion in Fig. 4 (1.189 MPa @ -17.4°) was adjusted, by calibration, to agree closely with the experimental phasor; the predicted phasor was determined by Fourier analyzing the simulated pressure variation.

Calibrating the pressure variation for given piston amplitude is approximately equivalent to calibrating the power for the following reason: The magnitude of the pressure and piston amplitude phasors, their relative phase, and the frequency of oscillation determine the power flowing from the compression space gas to the power piston, to the extent that the pressure and piston phasors accurately represent the actual piston amplitude and pressure variation. The equation used to calculate this power is:

$$\text{Power} = \pi \omega P_c A_{pis} X_p \sin \phi$$

Eq. (1) neglects the small effect of the buffer space on the power piston work; it shows that only the component of the pressure phasor which is 90° out of phase with the piston phasor (i.e.,  $P_c \sin \phi$ ) imparts usable power to the power piston.

Figure 4(a) shows how the various forces acting on the displacer add to yield the net displacer force required to produce the input motion. Shown are the net displacer force,  $M_d X_d$ , (as implied by the constrained displacer motion), the force due to the pressure acting on the displacer rod area,  $P_c A_{rod}$ , and the force due to the pressure drop,  $\Delta P A_{dis}$ ; an alternate representation of the sum of latter two forces is defined by:

$$\overrightarrow{P_c A_{rod}} + \overrightarrow{\Delta P A_{dis}} = \overrightarrow{P_e A_{rod}} + \overrightarrow{\Delta P (A_{dis} - A_{rod})}$$

The term on the right is a more natural representation of the forces acting on the displacer. However, since the compression space pressure is the pressure that is usually measured, the  $P_c A_{rod}$  phasor can be directly compared with test data (as shown in the figure.)

The two phasors,  $P_c A_{rod}$ , and,  $\Delta P A_{dis}$ , were determined by Fourier analysis of the simulated pressure drop and compression space pressure. The phasor,  $M_d \ddot{x}_d$ , was derived by differentiation of the displacer amplitude phasor,  $x_d$ . The gas spring force required to produce the displacer motion,  $x_d$ , is therefore determined by the following vector operation:

$$\vec{F}_{spring} = \vec{M}_d \ddot{x}_d - (\vec{P}_c A_{rod} + \vec{\Delta P A}_{dis})$$

This net spring force can then be resolved into the damping and spring components shown in the figure, that is:

$$\vec{F}_{spring} = \vec{C}_d \dot{x}_d + \vec{K}_d x_d$$

An alternate form of the displacer force diagram that is sometimes used is shown in Fig. 4(b). Here the phasors,  $P_c A_{rod}$ , and,  $\Delta P A_{dis}$  (of fig. 4(a)) have been summed to yield a "driving force" phasor. Thus the major damping force, that due to the pressure drop, does not appear explicitly and the "driving force" includes both driving and damping components. All other phasors are as shown in Fig. 4(a).

Figure 4(c) is identical to Fig. 4(a) except, the force phasors for the gas spring as simulated during the constrained motion run are substituted for the gas spring force phasors required to produce the constrained motion (The gas spring is simulated as a separate control volume with gas leakage from the spring and heat transfer to the walls of the spring.)

The simulated gas spring force phasor is seen to be somewhat different than the required one; the resulting net displacer force is too small. An attempt to adjust the gas spring parameters (leakage and heat transfer coefficient, not geometrical parameters) until the simulated spring phasor was the same as the required spring phasor, was not successful (reducing the gas spring leakage increased the magnitude of the phasor to approximately the right value but then the phase was not correct). (The gas spring simulation should be replaced with the option of either (1) gas spring simulation or (2) a linearized gas spring model which could be assigned the spring and damping constants required to give the desired gas spring force phasor. The linearized gas spring option would allow separation of the gas spring simulation and working space simulation problems during unconstrained motion.)

Figure 5 is the piston force phasor diagram for the constrained motion simulation. The three component phasors of the net piston

force,  $M_p \ddot{x}_p$ , are: the force due to the compression space pressure acting on the piston,  $P_c A_{pis}$ , the force due to the buffer space pressure,  $P_b A_{pis}$ , and the force due to the dashpot,  $C_{load} \dot{x}_p^2$ . The dashpot force phasor is a linearized representation of a very non-linear force; this probably explains the mismatch between the vector sum of the fundamentals of the three components and the fundamental of the net force.

The modeled load was calibrated against the experimental load by adjusting the dashpot load constant until the power dissipated by the dashpot agreed with the power flowing to the piston from the working space gas. This also resulted in good agreement of the simulated net piston force with the net piston force required to produce the constrained motion, as shown in Fig. 5.

Since the simulated gas spring of 4(c) is not equivalent to the required gas spring of 4(a), it is to be expected that an unconstrained simulation would produce different piston and displacer motions than measured (and used in the constrained motion simulation). Figure 6 shows this to be the case; it is a phasor diagram for an unconstrained simulation using Reference Case operating conditions. Here all the displacer force phasors were determined by the model. The amplitude and phase angles are seen to be somewhat different than for the constrained simulation of Fig. 4(a), but the difference is not great. Also, in this diagram there is seen to be a slight difference between the vector sum of the fundamentals of the three components and the fundamental of the net displacer force (The tips of phasors  $M_d \ddot{x}_d$  and  $\Delta P A_{dis}$  do not quite meet). This mismatch is an indication of the error involved in using a linearized model and/or the effect of model energy balance errors. The amplitude of the predicted pressure phasor is about 6 percent larger than the phasor determined from the test data; the predicted phase angle is within a degree of the test value. Piston and displacer amplitudes are in good agreement with the test data phasors of Fig. 4; the predicted displacer phase angle is about 4° smaller than the test value. Figure 7 shows the piston force diagram for the same unconstrained simulation of Fig. 6.

Table I compares experimental and predicted performance parameters for the Reference experimental run and the constrained and unconstrained simulations of this run (for which force diagrams are shown in fig. 4 through 7). For the unconstrained run, predicted indicated power as determined by integrating the pressure-volume "diagram," is higher than the measured value by almost 12 percent (although the predicted and measured

powers calculated from the phasor diagram of Fig. 6 are in almost perfect agreement). Predicted heat input is low by almost 3 percent and predicted efficiency is high by almost 15 percent. Cycle energy balance errors were found to increase with increased leakage flows. The power piston energy balance error (of the unconstrained simulation) can be reduced by reducing the size of the time increment used in the numerical integrations.

Figure 8 is a displacer force diagram generated by Sunpower for comparison with NASA experimental Run #334, which had the same engine operating conditions as the Reference Case run. Sunpower used the procedure of Fourier analyzing the Run #334 piston and displacer motions and inputting these motions to their RE1000 model. Apparently, by simulating the gas spring characteristics required to yield the measured displacer motion, Sunpower achieved essentially identical results for constrained and unconstrained simulations. Comparison of Fig. 4(a) and 8 shows there was some difference in measured displacer phase angles ( $4^\circ$  to  $5^\circ$ ) and displacer amplitudes. Even so, the resulting pressure phasors for the two runs are seen to be in close agreement. Sunpower's simulation predicted a larger pressure drop (at a smaller phase angle). The assumed displacer gas spring constant (fig. 8) was about 30 percent larger than the required gas spring constant of the NASA model.

Implicit in the use of these phasor diagrams is the assumption that the dynamics of the engine model (and the engine) can be approximated by the dynamics of a linear 2nd order system of equations. The facts that:

(a) for the experimental data, the fundamentals of the measured piston and displacer amplitudes and pressure are much larger than the higher order harmonics

(b) for the model predictions, the vector sums of the fundamentals of the various displacer and piston force components are close approximations of the fundamentals of the net displacer and piston forces support this assumption. Rauch shows in Ref. 9 that a complete engine model can be based on harmonic analysis of Stirling engine variables.

#### COMPARISON OF PREDICTIONS WITH A RANGE OF EXPERIMENTAL DATA

With the free-piston model thus calibrated against the Reference experimental run, it was assumed sufficiently accurate for comparison with a wider range of experimental

data. Experimental runs used for this purpose were #336 to #341; these were for various dashpot loads with nominal operating conditions of heater temperature =  $650^\circ\text{C}$ , cooling water inlet temperature =  $30^\circ\text{C}$  and mean pressure = 7.0 MPa (1015 psi). Other experimental runs used were #312 to #317; for these runs the heater temperature was reduced to  $450^\circ\text{C}$ . Cooling water temperature and the mean pressure were unchanged. The experimental performance parameters for these runs are compared with predicted performance over the same load range in Fig. 9 through 16.

Comparisons of measured and predicted power and efficiency are shown in Fig. 9 and 10. A range of piston strokes was produced by varying engine load; the model load was changed by varying the dashpot load constant. Comparisons are shown for a range of loads at heater temperatures of  $650^\circ\text{C}$  and  $450^\circ\text{C}$ . Cooler tube temperature was set equal to experimental coolant inlet temperature for all model predictions. Mean pressure was 7.0 MPa (1015 psi).

The greatest difference between predicted and experimental values of power and efficiency is seen to occur at the largest strokes and the lowest heater temperature. The increasing deviation between measured and predicted values with increasing stroke may be the result of deficiencies in the present cooler model, as discussed below.

Predictions of piston and displacer strokes are seen to be in good agreement over most of the tested load range (fig. 11). Figure 12 shows that predicted displacer-piston phase is low by from 8 to 13 degrees over the range of loads and temperatures tested. Figure 13 shows that predicted piston-pressure phase angle is not as sensitive to engine load as the test data indicates it should be. Figure 14 shows that predicted engine frequency is too sensitive to engine load; the test data shows that frequency is almost constant over the load range tested.

Figure 16 compares measured and predicted average gas temperatures for the compression space, at the  $650^\circ\text{C}$  heater temperature (results were similar for the  $450^\circ\text{C}$  cases). This plot can be contrasted with the expansion space average gas temperature comparison in Fig. 15. The predicted average gas temperature in Fig. 16 does not change as much with stroke as does the measured value; this may be because the cooler wall temperature is held constant rather than calculating it from the coolant inlet temperature and the heat transferred out via the cooler. This greater difference between measured and predicted compression space gas temperatures at the larger strokes may also explain the

increased difference between measured and predicted, power and efficiency at the higher strokes (figs. 9 and 10).

#### CONCLUDING REMARKS

Predicted power and efficiency are in reasonably good agreement with test data for the calibrated model. The results suggest that improvements to the cooler model and addition of an appendix gap loss calculation should improve the agreement between predictions and data and, perhaps, reduce the amount of calibration required.

Two changes should be made to the cooler model:

1. A rectangular passage heat transfer correlation should be substituted for the tube heat transfer correlation.

2. The water side of the cooler should be modeled (Coolant inlet temperature would be input instead of cooler wall temperature).

Sunpower predicts an appendix gap pumping loss of about 200 W for the Run #334 engine operating conditions; this loss should be included in the Lewis RE1000 model calculation. A relationship has been noted between errors in the model energy balance and the amount of power piston leakage; an effort should be made to improve this energy balance.

Several different possible leakage paths exists for (1) leakage by the power piston and (2) leakage to and from the gas spring. Only one path is considered for each of the above leakages in the current model. The leakage paths modeled should be re-evaluated to ensure that the simulated leakages are reasonable representations of the actual ones.

Current plans are to compare the model against additional sets of test data and continue development, as required. The engine has now been tested with two different displacers and two different regenerator matrixes; this data is available for model validation. A hydraulic output load device is being designed and built for the RE1000 engine; these tests should provide additional data for model validation.

#### REFERENCES

1. Tew, Roy; Jefferies, Kent; and Miao, David: "A Stirling Engine Computer Model for Performance Calculations," DOE/NASA/1011-78/24, NASA TM-78884, July 1978.
2. Tew, Roy C. Jr; Thieme, Lanny G.; and Miao, David: "Initial Comparison of Single Cylinder Stirling Computer Model Predictions with Test Results," DOE/NASA/1040-78/30, NASA TM-79044, February 1979.
3. Dochat, George; Moynihan, Thomas; and Dahr, Manmohan: "1 Kw Free-Piston Stirling Engine/Linear Alternator Test Program," Paper 809400, Proceedings of 15th Intersociety Energy Conversion Engineering Conference, August 1980.
4. Giansante, Joseph E.: "A Free Piston Stirling Engine Performance Code," Final Report for Contract 8NAS3-21277, Mechanical Technology, Inc. Document 81TR17, November 1980.
5. Schreiber, Jeff: "Testing and Performance Characteristics of a 1 Kw Free Piston Stirling Engine," NASA TM-82999, April 1983.
6. Schreiber, Jeffrey: "Test Results and Description of 1 Kw Free-Piston Stirling Engine with a Dashpot Load," DOE/NASA/1005-1, NASA TM-83407, August 1983.
7. Tew, Roy C.: "Computer Program for Stirling Engine Performance Calculations," DOE/NASA/51040-42, NASA TM-82960, January 1983.
8. Knoll, Richard H.; Tew, Roy C. Jr.; and Klann, John L.: "Downsizing Assessment of Automotive Stirling Engines," DOE/NASA/1040-49, NASA TM-83468, September 1983.
9. Rauch, J. S.; "Harmonic Analysis of Stirling Engine Thermodynamics," Paper 809335, Proceedings of 15th Energy Conversion Engineering Conference, August 1980.



TABLE I. - COMPARISON OF RE1000 PREDICTED AND EXPERIMENTAL PERFORMANCE

Run description	Frequency, $\omega$ , Hz	Heat input, kW	Heat rejected, kW	Piston Power		Dashpot power dissipation, kW	Indicated <sup>a</sup> efficiency	Cycle <sup>b</sup> energy balance error percent	Power Piston <sup>c</sup> energy balance error percent
				Indicated PdV, kW	Phasor diag. $\pi \omega P_c A_p \sin \phi$				
Experimental predicted:	30.4	3.404	2.421	0.983	1.075	1.024	0.289	0.0	4.17
Constrained	30.4	3.517	2.240	1.141	1.137	1.146	.324	-3.88	
Unconstrained	30.2	3.313	2.104	1.097	1.071	1.121	.331	-3.38	2.19

<sup>a</sup>Indicated efficiency  $\frac{\text{Indicated power}}{\text{Heat input}}$

<sup>b</sup>Cycle energy balance error  $\frac{\text{Indicated power} + \text{heat rejected}}{\text{Heat input}}$

<sup>c</sup>Power piston energy balance error  $\frac{\text{Dashpot power dissipation}}{\text{Indicated power}}$

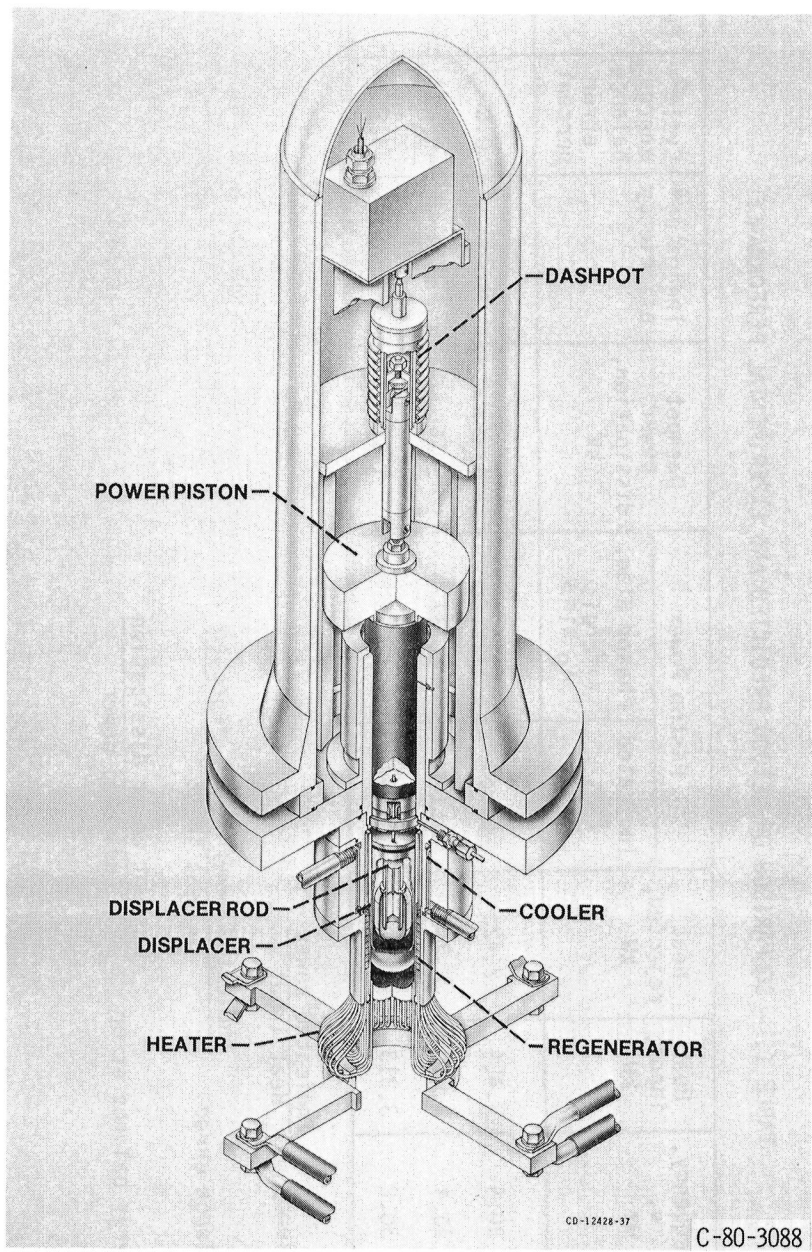


Figure 1. - Cutaway view of RE-1000 free-piston, free-displacer Stirling Engine.

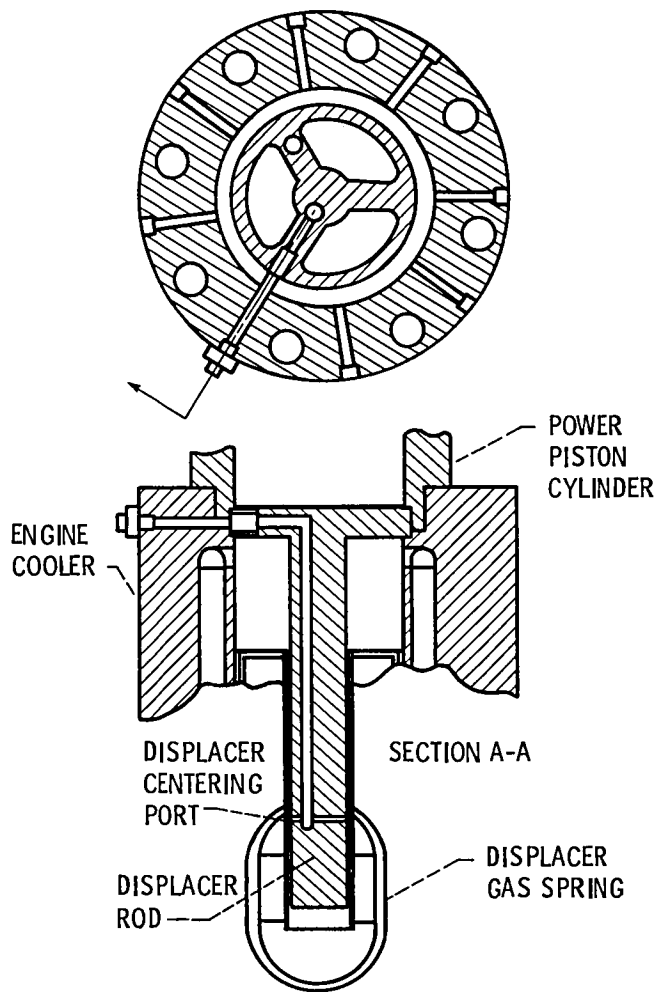


Figure 2. - Displacer rod mounting and communication ports for RE-1000 engine.

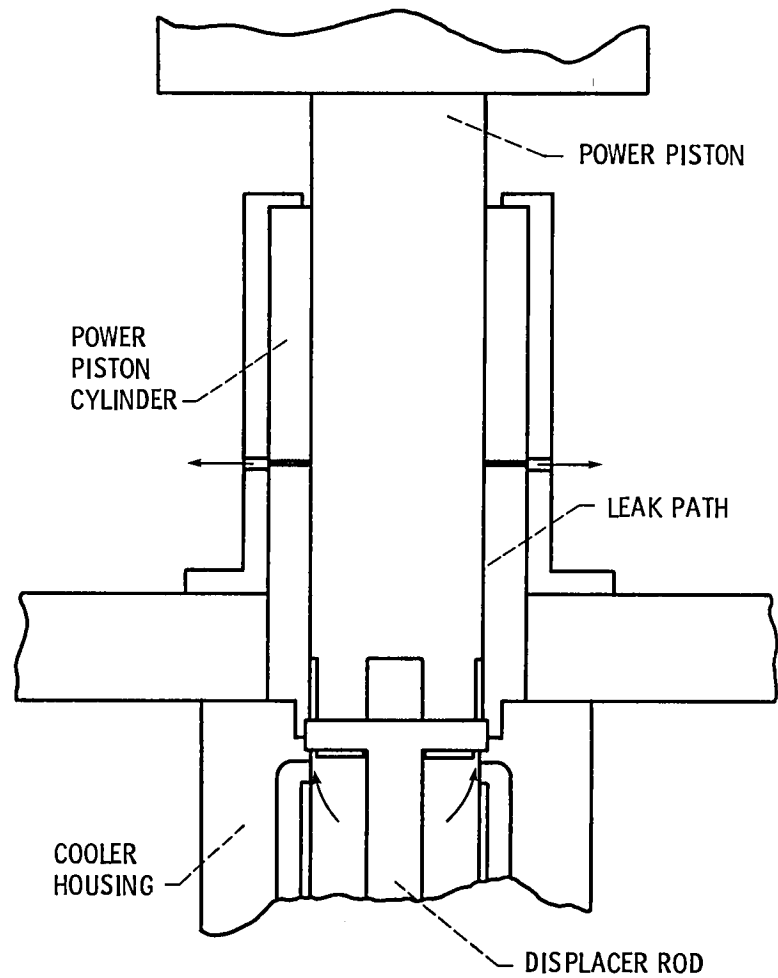
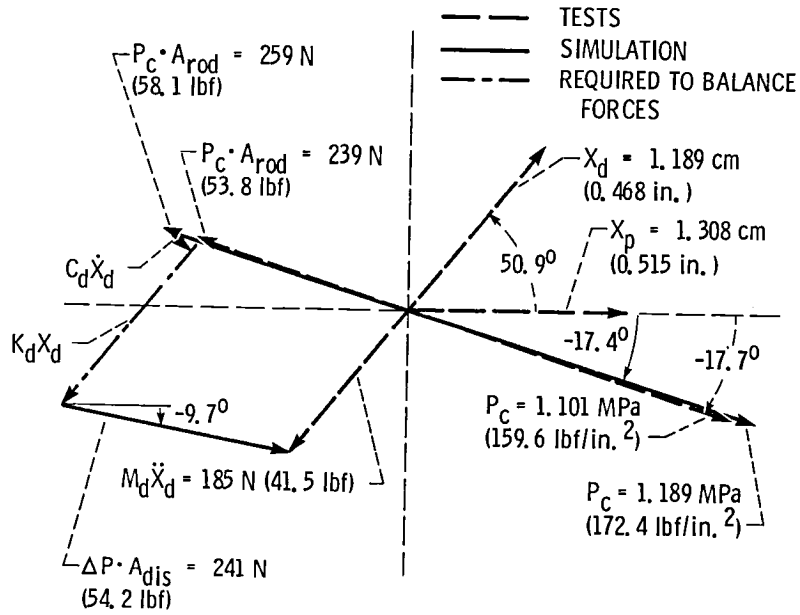
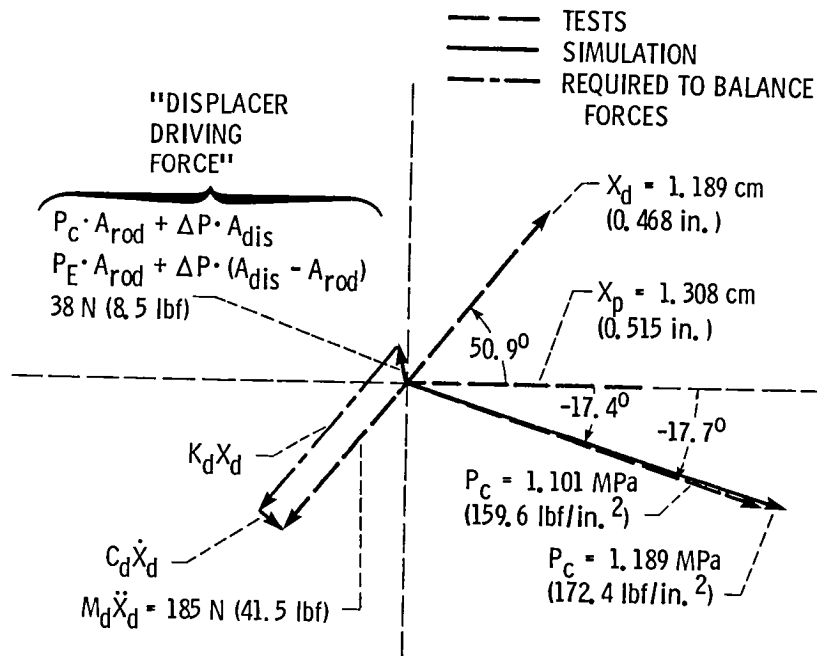


Figure 3. - Power piston leak path of RE-1000 engine.



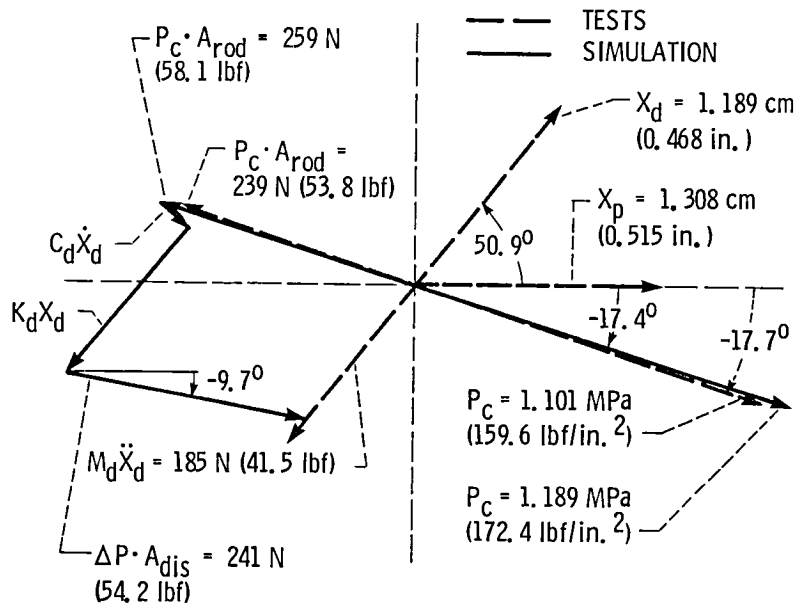
(a) Required components of gas spring force: damping component,  $C_d \dot{X}_d = 30 \text{ N (6.7 lbf)}$ ; spring component,  $K_d X_d = 207 \text{ N (46.6 lbf)}$ .

Figure 4. - Displacer phasor diagram - constrained motion (reference case).



(b) Required components of gas spring force: spring component,  $K_d X_d = 207 \text{ N (46.6 lbf)}$ ; damping component,  $C_d \dot{X}_d = 30 \text{ N (6.7 lbf)}$ .

Figure 4. - Continued.



(c) Simulated gas spring force components: damping component,  $C_d \dot{X}_d = 37 \text{ N}$  (8.3 lbf); spring component,  $K_d X_d = 184 \text{ N}$  (41.3 lbf).

Figure 4. - Concluded.

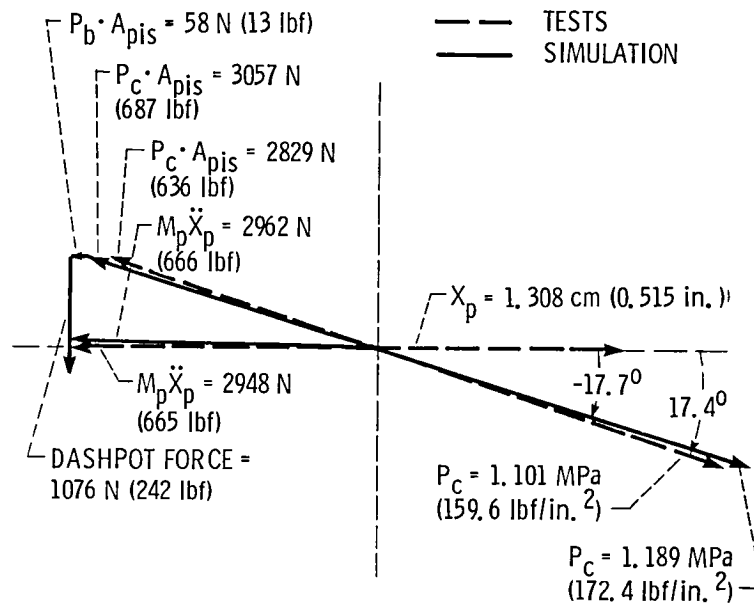


Figure 5. - Piston phasor diagram - constrained motion (reference case).

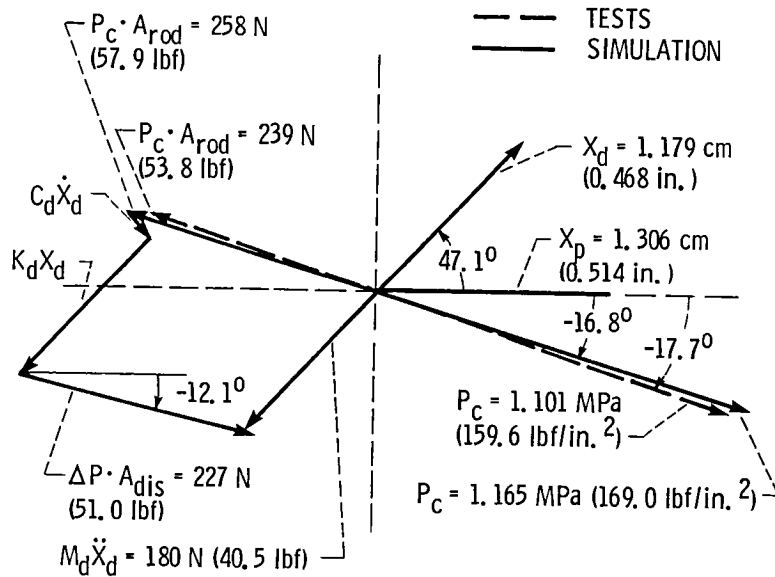


Figure 6. - Displacer phasor diagram - unconstrained motion (reference case). Gas spring force components: damping component,  $C_d \dot{X}_d = 32 \text{ N}$  (7.3 lbf); spring component,  $K_d X_d = 185 \text{ N}$  (41.6 lbf).

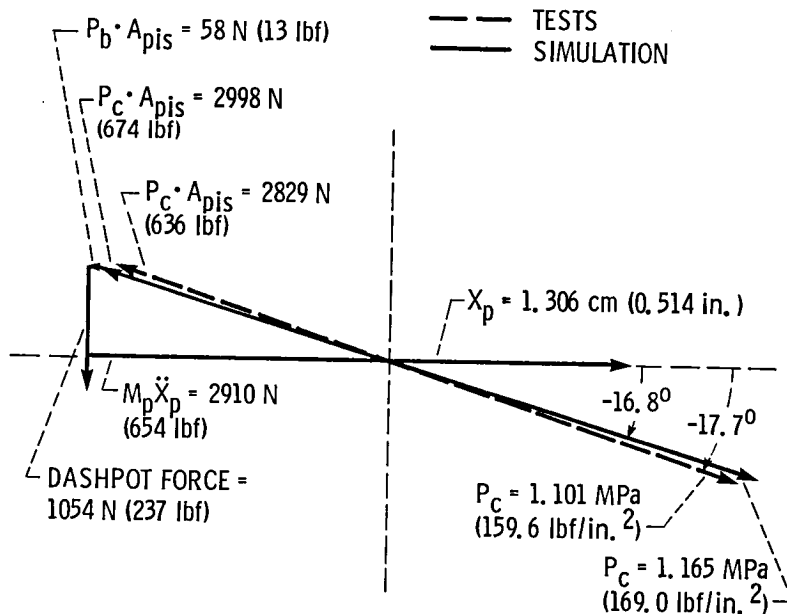


Figure 7. - Piston phasor diagram - unconstrained motion (reference case). Test frequency, 30.4 Hz; simulated frequency, 30.2 Hz.

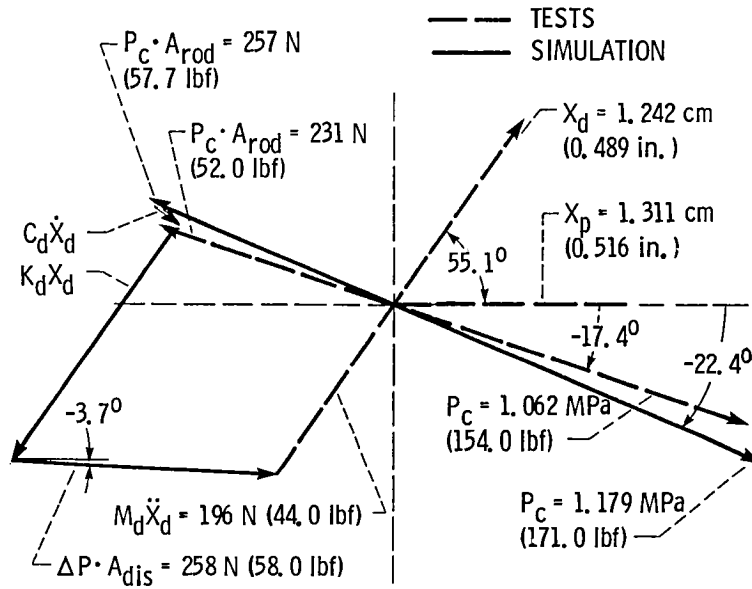


Figure 8. - Sunpower simulation of Lewis RE1000 test run number 334. Test frequency, 30.6 Hz. Gas spring force components: damping component,  $C_d \dot{X}_d = 32 \text{ N}$  (7.1 lbf); spring component,  $K_d X_d = 272 \text{ N}$  (61.1 lbf).

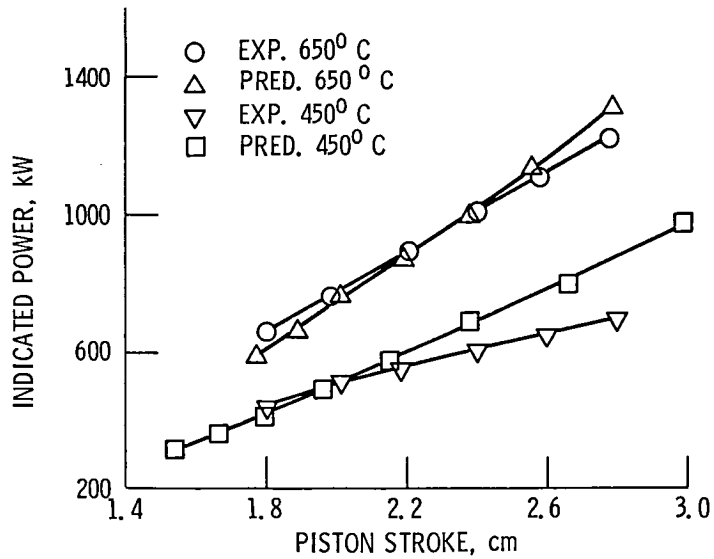


Figure 9. - Power as function of piston stroke RE1000 engine.

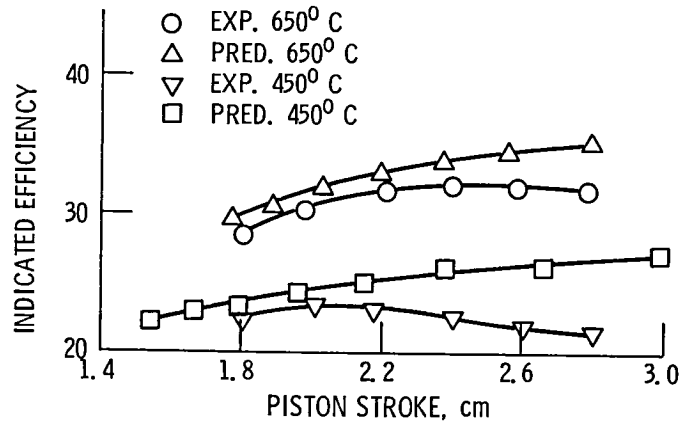


Figure 10. - Efficiency as function of piston stroke RE1000 engine.

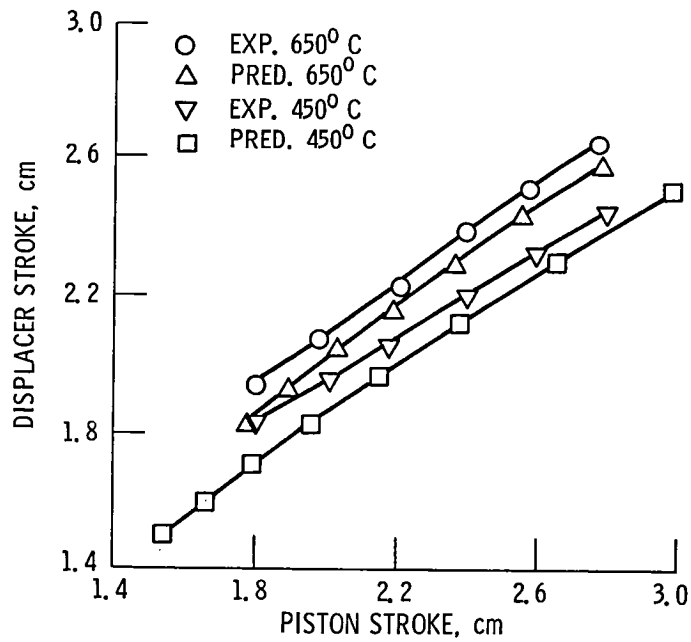


Figure 11. - Displacer stroke as function of piston stroke RE1000 engine.

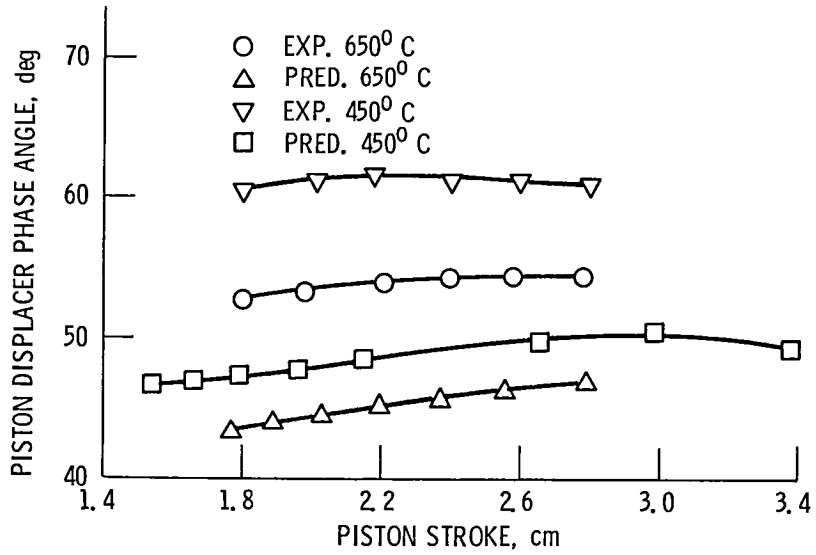


Figure 12. - Piston displacer phase angle as function of stroke RE1000 engine.

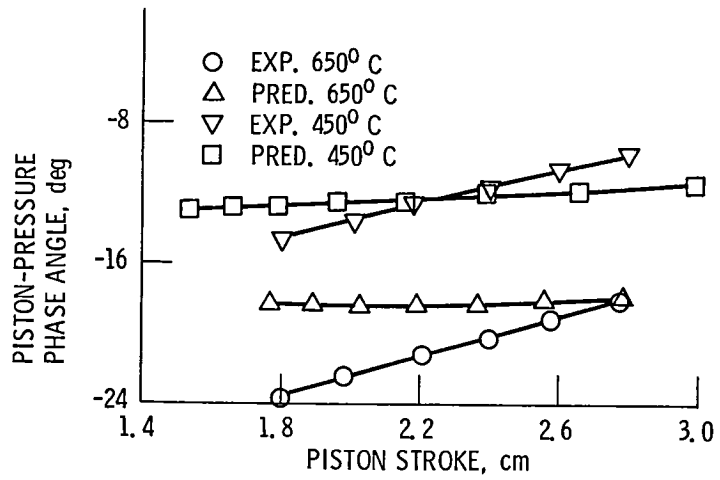


Figure 13. - Piston-pressure phase as function of piston stroke RE1000 engine.

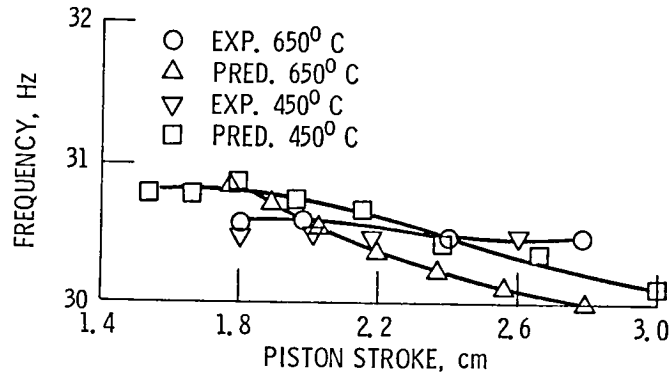


Figure 14. - Engine speed as function of piston stroke RE1000 engine.

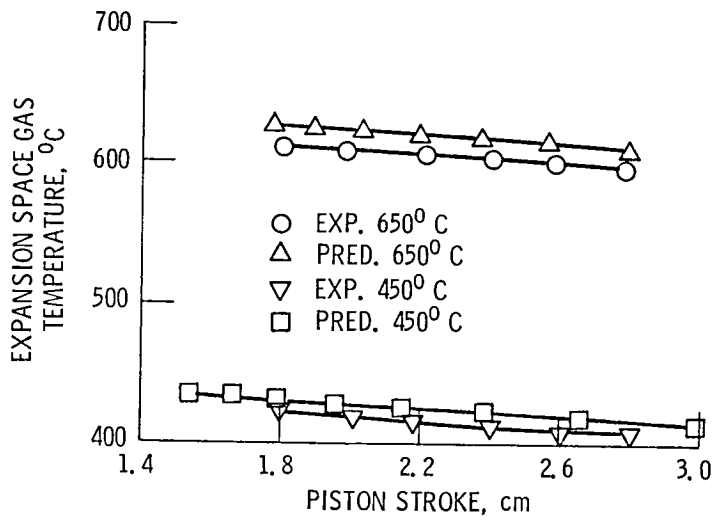


Figure 15. - Expansion space gas temperature as function of stroke RE1000 engine.

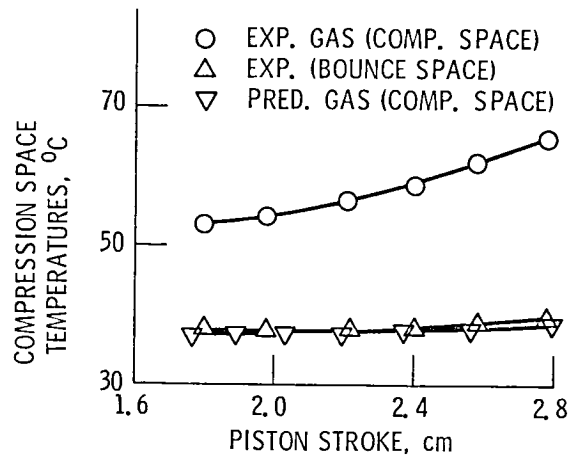


Figure 16. - Compression space temperatures as function of stroke RE1000 engine (heater temperature, 650°C).



1. Report No. NASA TM-83650		2. Government Accession No.		3. Recipient's Catalog No.	
4. Title and Subtitle Comparison of Free-Piston Stirling Engine Model Predictions With RE1000 Engine Test Data				5. Report Date	
				6. Performing Organization Code 778-16-12	
7. Author(s) Roy C. Tew				8. Performing Organization Report No. E-2095	
				10. Work Unit No.	
9. Performing Organization Name and Address National Aeronautics and Space Administration Lewis Research Center Cleveland, Ohio 44135				11. Contract or Grant No.	
				13. Type of Report and Period Covered Technical Memorandum	
12. Sponsoring Agency Name and Address U.S. Department of Energy Division of Building and Community Systems Washington, D. C. 20545				14. Sponsoring Agency Code Report No. DOE/NASA/1005-3	
15. Supplementary Notes Prepared under Interagency Agreement DE-AI05-82OR1005. Prepared for Nineteenth Intersociety Energy Conversion Engineering Conference cosponsored by the ANS, ASME, SAE, IEEE, AIAA, ACS, and AIChE San Francisco, California, August 19-24, 1984.					
16. Abstract Predictions of a free-piston Stirling engine model are compared with RE1000 Sunpower engine test data taken at NASA-Lewis Research Center. The model validation and the engine testing are being done under a joint interagency agreement between the Department of Energy's Oak Ridge National Laboratory and NASA-Lewis. A kinematic code developed at Lewis was upgraded by Mechanical Technology, Inc. to permit simulation of free-piston engine performance; it was further upgraded and modified at Lewis and is currently being validated. The model predicts engine performance by numerical integration of equations for each control volume in the working space. Piston motions are determined by numerical integration of the force balance on each piston or can be specified as Fourier series. In addition, the model Fourier analyzes the various piston forces to permit the construction of phasor force diagrams. The paper compares predicted and experimental values of power and efficiency and shows phasor force diagrams for the RE1000 engine displacer and piston. Further development plans for the model are also discussed.					
17. Key Words (Suggested by Author(s)) Stirling engines Computer model Power systems Energy conversions			18. Distribution Statement Unclassified - unlimited STAR Category 85 DOE Category UC-96		
19. Security Classif. (of this report) Unclassified		20. Security Classif. (of this page) Unclassified		21. No. of pages	22. Price* A02



National Aeronautics and  
Space Administration

Washington, D.C.  
20546

Official Business  
Penalty for Private Use, \$300

SPECIAL FOURTH CLASS MAIL  
BOOK



Postage and Fees Paid  
National Aeronautics and  
Space Administration  
NASA-451



POSTMASTER: If Undeliverable (Section 154  
Postal Manual) Do Not Return

UNITED STATES DEPARTMENT OF ENERGY  
P.O. BOX 62  
OAK RIDGE, TENNESSEE 37830  
OFFICIAL BUSINESS  
PENALTY FOR PRIVATE USE, \$300

POSTAGE AND FEES PAID  
UNITED STATES  
DEPARTMENT OF ENERGY



0986

NATIONAL AERONAUTICS AND SPACE ADM  
ATTN LIBRARY  
LANGLEY RESEARCH CENTER  
HAMPTON, VA 23665